

Decoherence in a spin–spin-bath model with environmental self-interaction

L. Tessieri and J. Wilkie

*Department of Chemistry, Simon Fraser University,
Burnaby, British Columbia, Canada V5A 1S6*

11th September 2002

Abstract

A low temperature model system consisting of a central spin coupled to a spin-bath is studied to determine whether interaction among bath spins has an effect on central spin dynamics. In the absence of intra-environmental coupling, decoherence of the central spin is fast and irreversible. Strong intra-environmental interaction results in an effective decoupling of the central spin from the bath and suppression of decoherence. Weaker intra-environmental coupling reduces but does not eliminate decoherence. We believe that similar behaviour will be observed in any system with a self-interacting environment.

PACS numbers: 03.65.Yz, 03.67.Lx, 05.30.-d

1 Introduction

Exact theories for the dynamics of open quantum systems require solution of the Schrödinger equation (or an equivalent formalism) for the full system plus environment degrees of freedom. This is impossible to do analytically except when the environment consists of a set of independent harmonic oscillators (e.g., Caldeira-Leggett model [1], spin-boson model [2]) or spins [3]. Neglect of intra-environmental coupling is thus strongly motivated by reasons of mathematical convenience. The purpose of the present study is to

determine whether this approximation is justified physically. Our model consists of a small (i.e., highly quantum) central spin interacting with a bath of self-interacting spins representing the degrees of freedom of the environment. We shall sometimes refer to this central spin as the subsystem.

Intuition suggests that coupling between environment degrees of freedom can significantly affect the properties of the bath and consequently, through subsystem-environment coupling, the dynamics of the central spin. Mutual interactions of the bath modes allow energy exchange without using the subsystem as an intermediary. Consider an initial state of the subsystem-environment which is perturbed away from equilibrium. With intra-environmental coupling the rapid initial flow of energy toward a new equilibrium state will largely occur within the environment. Without intra-environmental coupling the energy must flow through the subsystem, leaving it strongly entangled with the bath and hence badly decohered. [Note that the decoherence effects discussed in this manuscript differ greatly from those which affect macroscopic subsystems [4].]

Intra-environmental interactions may also alter more abstract properties of the bath. The classical dynamics of a bath of oscillators can change from regular to chaotic when non-linear interactions are added [5]. In the quantum case, such coupling modifies the statistical properties of the energy levels and eigenstates of the bath. Specifically, the energy spectra of quantum systems with chaotic classical counterpart exhibit level repulsion, while systems with regular dynamics in the classical limit show a clustering of the energy levels [6]. The structure of the bath eigenstates also changes when the dynamics of the bath undergoes a transition from regular to chaotic. This effect can be analysed by considering the form of the Wigner functions of energy eigenstates: for chaotic systems the Wigner functions spread more or less uniformly over the energetically available phase space [7], whereas in the case of regular systems they are more lumpy. Moreover, these spectral signatures of chaos have dynamical consequences [8]. It is therefore reasonable to expect that dissipation and decoherence will assume different forms for coupled and uncoupled baths.

A qualitative understanding of the effects of bath self-interaction on decoherence, while of obvious theoretical interest, might also have important applications. Minimization of decoherence is essential for the development and implementation of a number of new technologies such as quantum computing [9], laser control of chemical reactions [10] and molecular electronics [11]. For quantum computing some proposed physical platforms, such as

laser manipulated cold ions in traps in near vacuum [12] can very effectively minimise decoherence. Whether such platforms can be scaled to the 10^5 ions needed to perform useful computations like factorisation of large integers is unclear [12]. Proposed solid state platforms such as single-electron quantum dots embedded in a semiconductor [13] are readily scaleable [14], but decoherence is a serious obstacle. In principle decoherence and dissipation can be reduced through judicious choice of states for implementation of the qubit [15]. (A trivial example would be to avoid states with electric-dipole allowed transitions.) Since the solid state in principle provides enormous freedom over the choice of qubit and matrix, further theoretical insight into the mechanisms of decoherence might prove extremely useful in selecting optimal configurations.

The effect of environmental self-interaction is almost certainly of importance in the solid state. Unfortunately, as we noted above, the analysis of the mechanisms of decoherence and dissipation in self-interacting environments is a problem that defies exact analytical treatments. Standard approaches, like the Feynman-Vernon influence functional method [16] or the Nakajima-Zwanzig projection technique [17] cannot be successfully applied unless restrictive hypotheses are made on the nature of the bath and its coupling to the subsystem of interest. Thus, for exact results we must rely on what we can calculate numerically. Environments with few degrees of freedom should in principle provide much of the qualitative information we seek. Such numerical studies also serve a second purpose, namely to provide exact results which can be used as a touchstone to test the reliability of the approximate analytical methods which describe open systems (e.g., Redfield [18], SRA [19] master equations and other approaches [20]).

In this paper we study numerically and without approximation the dynamics of a spin-1/2 subsystem coupled to a bath of N *interacting* spin-1/2 modes. While spin-spin-bath models have been previously studied [3, 21] intra-environmental coupling has been neglected. Many different physical systems can be represented with such a model. Examples include a spin chain, a set of magnetic impurities in a solid [13] or an array of magnetic moments in a molecular crystal. Alternatively, the system can be interpreted as a model of an atomic impurity in a crystalline solid at low temperature. The impurity is vibronically coupled to a bath consisting of the phonon modes of the solid [22]. At low temperatures, the probability that the impurity is in an electronic state other than the ground state is negligible. However, the impurity can be prepared in a chosen (non-radiative) excited state and so is

effectively a two-level system. By the same token, in the low-temperature limit the phonon modes reduce to oscillators with only two accessible levels and can therefore be described as spin-1/2 modes (i.e., $a^\dagger a \rightarrow \sigma_z$, $a^\dagger + a \rightarrow \sigma_x$, etc.). Jahn-Teller interactions couple the central spin to the bath. Phonon-phonon interactions inter-couple the bath spins. In our study we consider both ferromagnetic and antiferromagnetic interactions.

We show that environmental self-interaction has an extremely important effect on decoherence. Strong intra-environmental interactions effectively decouple the subsystem from the environment, and even weak interactions qualitatively change the manner in which phase information is lost. We see no reason to suppose the effect is peculiar to the spin-spin-bath model, and it should prove of importance in areas of physics where preservation of quantum interference is paramount.

Section 2 explains our model in detail. In section 3 we outline the numerical methods we employ to solve the subsystem dynamics. Numerical results for subsystem dynamics are discussed in detail in section 4 for a wide range of intra-environmental couplings. We summarise our findings in section 5 and discuss their relevance for more general environments.

2 The spin-spin-bath model

In mathematical terms, our model is defined by the Hamiltonian

$$H = H_0 + H_B + H_I \tag{1}$$

where

$$H_0 = \frac{\hbar\omega_0}{2}\sigma_z^{(0)} + \beta\sigma_x^{(0)} \tag{2}$$

is the Hamiltonian of the central spin (denoted by the superscript 0),

$$H_B = \sum_{i=1}^N \frac{\hbar\omega_i}{2}\sigma_z^{(i)} + \beta \sum_{i=1}^N \sigma_x^{(i)} + \lambda \sum_{i=1}^{N-1} \sum_{j=i+1}^N \sigma_x^{(i)}\sigma_x^{(j)} \tag{3}$$

is the Hamiltonian of the bath, and

$$H_I = \lambda_0 \sum_{i=1}^N \sigma_x^{(i)}\sigma_x^{(0)} \tag{4}$$

describes the interaction between the central spin and its environment. For simplicity, in the rest of this paper we adopt a system of units such that $\hbar = 1$. Note that the terms proportional to β and λ in Hamiltonians (3) represent anharmonic phonon-phonon interactions or non-linear spin interactions, depending on which interpretation of the model one has in mind.

To complete the definition of the model, we have to specify the values of the various parameters which appear in the Hamiltonian. We assume that the frequencies of the bath spins are positive random variables with the Debye probability density

$$p(\omega) = \begin{cases} 3\omega^2/\omega_c^3 & \text{for } 0 < \omega < \omega_c \\ 0 & \text{for } \omega_c < \omega \end{cases} \quad (5)$$

appropriate for the low energy acoustic modes of a crystal. This is equivalent to saying that the bath has an Ohmic spectral density with a sharp cut-off at $\omega = \omega_c$ which is not necessarily the Debye frequency itself. At the temperatures we consider, modes with large frequency are unlikely to be populated and so it makes sense to choose a smaller ω_c to reflect this fact. For the frequency of the central spin, we arbitrarily chose the value $\omega_0 = 0.8288\omega_c$. Note that the results obtained in this manuscript do not depend crucially on the specific form (5) of the frequency distribution. In fact, we repeated our calculations with the box distribution

$$p(\omega) = \begin{cases} 1/\omega_c & \text{for } 0 < \omega < \omega_c \\ 0 & \text{for } \omega_c < \omega \end{cases}$$

and found the qualitative behaviour of the model unaltered by the change.

To simplify the form of mathematical expressions, we set $\omega_c = 1$, $\lambda_0 = 1$, and we varied the relative strength of the intra-environmental interactions by letting the parameter λ range in the interval from $\lambda = 0$ (bath without internal spin-spin coupling) to $\lambda = 10$ (strong bath self-interaction). In addition to considering positive values of λ , which correspond to antiferromagnetic interactions, we investigated the case of ferromagnetic couplings, letting λ assume negative values in the interval $[-10, 0]$.

We set $\beta = 0.01$. An important consequence of the fact that β , although small, is not zero, is that the Hamiltonian (1) cannot be reduced to block form. To understand this point, we observe that the Hilbert space of the

system (1) is spanned by the vectors

$$\begin{aligned}
|0\rangle &= |0\rangle_N |0\rangle_{N-1} \dots |0\rangle_1 |0\rangle_0 \\
|1\rangle &= |0\rangle_N |0\rangle_{N-1} \dots |0\rangle_1 |1\rangle_0 \\
|2\rangle &= |0\rangle_N |0\rangle_{N-1} \dots |1\rangle_1 |0\rangle_0 \\
&\vdots \\
|2^{N+1} - 1\rangle &= |1\rangle_N |1\rangle_{N-1} \dots |1\rangle_1 |1\rangle_0
\end{aligned} \tag{6}$$

where the symbols $|1\rangle_i$ and $|0\rangle_i$ denote the ‘up’ and ‘down’ states of the i -th spin, i.e., the eigenstates of the Pauli z -spin matrix $\sigma_z^{(i)}$ with eigenvalues $+1$ and -1 respectively. Note that the basis states (6) can be conveniently interpreted as binary representations of integer numbers ranging from 0 to $2^{N+1} - 1$ if the vector

$$|k_N, k_{N-1}, \dots, k_0\rangle = |k_N\rangle_N |k_{N-1}\rangle_{N-1} \dots |k_0\rangle_0 \tag{7}$$

(with $k_i = 0, 1$ for $i = 0, \dots, N$) is associated to the integer

$$k = k_0 + 2k_1 + \dots + 2^N k_N = \sum_{n=0}^N 2^n k_n. \tag{8}$$

For $\beta = 0$ the Hamiltonian (1) can be reduced to block form by regrouping the basis vectors (6) in two sets defined by the condition that the states of each set have an even or odd number of spins ‘up’. In fact, for $\beta = 0$ all terms of the Hamiltonian (1) have the effect of flipping either zero or two spins at once, thereby leaving invariant the subspaces spanned by the ‘even’ and ‘odd’ basis states. The terms proportional to β , on the other hand, flip just one spin and therefore connect the ‘even’ and ‘odd’ subspaces, making the Hamiltonian (1) irreducible.

3 Numerical approach

Assume that the bath is initially in thermal equilibrium at temperature T and that the central spin is in the excited state $|1\rangle_0$. [In the case of an impurity in an insulating solid such an initial state could be prepared using a fast laser pulse with a frequency matching a transition of the impurity but lying in the crystal’s band gap.] The initial density matrix of the whole system therefore has the product form

$$\rho(0) = \rho_0(0) \otimes \rho_B(0), \tag{9}$$

with

$$\rho_0(0) = |1\rangle_{00}\langle 1| \quad \text{and} \quad \rho_B(0) = (1/Q) \exp(-H_B/kT)$$

where $Q = \text{Tr}_B [\exp(-H_B/kT)]$. After introducing the notation

$$H_B |\phi_n^{(B)}\rangle = E_n |\phi_n^{(B)}\rangle \quad (10)$$

for the 2^N eigenvalues and eigenvectors of the bath Hamiltonian and

$$|\psi_n(0)\rangle = |1\rangle_0 \otimes |\phi_n^{(B)}\rangle \quad (11)$$

for the corresponding initial conditions of the total system, we can write the initial density matrix (9) in the form

$$\rho(0) = \sum_{n=1}^{2^N} |\psi_n(0)\rangle \frac{e^{-E_n/kT}}{Q} \langle \psi_n(0)|.$$

To study the dynamics we have determined the states

$$|\psi_n(t)\rangle = \exp(-iHt) |\psi_n(0)\rangle \quad (12)$$

which evolve from (11). Once states (12) are known the evolved density is constructed via

$$\rho(t) = \exp(-iHt) \rho(0) \exp(iHt) = \sum_{n=1}^{2^N} |\psi_n(t)\rangle \frac{e^{-E_n/kT}}{Q} \langle \psi_n(t)|, \quad (13)$$

and the reduced density of interest is

$$\rho_0(t) = \text{Tr}_B [\rho(t)] = \sum_{n,m} \langle \phi_m^{(B)} | \psi_n(t) \rangle \frac{e^{-E_n/kT}}{Q} \langle \psi_n(t) | \phi_m^{(B)} \rangle. \quad (14)$$

We used two complementary techniques to compute the dynamics (12). For small baths, $N \leq 11$, we numerically diagonalised both the bath Hamiltonian (3) and the total Hamiltonian (1) using standard Householder routines (see Ref. [23]). This method gives the exact reduced density at all times and allows us to consider a range of temperature. However, it cannot be used for baths composed of a large number N of spins since matrices of size $2^N \times 2^N$ quickly exceed computer resources. For large baths with $N \geq 12$ spins, we exploited the low-temperature limit. For $kT \rightarrow 0$, high-energy eigenstates of

the bath are depleted and one can truncate the sum in Eq. (13) to the first M terms, with $M \ll 2^N$, so that the density matrix takes the form

$$\rho(t) \simeq \sum_{n=1}^M |\psi_n(t)\rangle \frac{e^{-E_n/kT}}{Q} \langle \psi_n(t)|. \quad (15)$$

Thus a complete diagonalisation of the bath Hamiltonian becomes unnecessary. We chose a bath temperature of $kT = 0.02$ for which the number of terms M needed in (15) is 20. We checked that neglected terms were irrelevant by evaluating the probability that the bath be in an eigenstate of energy $E > E_{20}$. For baths with $N \leq 11$ spins with $0 \leq \lambda \leq 10$ we obtained an upper bound

$$P(E_B > E_{20}) = 1 - \sum_{n=1}^{20} e^{-E_n/kT} / Q < 10^{-4},$$

showing that bath eigenstates with $E > E_{20}$ are unpopulated. As a further check, for baths composed of more than 11 spins we estimated the ratio $R = p_{20}/p_1 = \exp(E_1 - E_{20})$. For $N = 14$, $0 \leq \lambda \leq 10$ and $kT = 0.02$ the probability ratio was less than 10^{-6} .

To determine the M bath eigenstates of lowest energy, we used ARPACK routines based on the Lanczos algorithm(see [24]). Evolved states (12) were calculated using a Runge-Kutta algorithm of eighth order [25]. Neither the programs for the partial diagonalisation of the bath Hamiltonian, nor the Runge-Kutta subroutine required that the whole Hamiltonian matrix be stored in the computer memory, but only that the matrix-vector product $H|\psi\rangle$ be defined. This more efficient use of computer resources allowed us to consider baths of up to 14 spins.

We calculated $H|\psi\rangle$ given an input state $|\psi\rangle$ by iterated calls to subroutines which multiplied by $\sigma_x^{(i)}$ and $\sigma_z^{(i)}$. Consider multiplication by $\sigma_x^{(i)}$ as an example. With vectors (6) as a basis for our Hilbert space

$$\sigma_x^{(i)}|\psi\rangle = \sum_{k=0}^{2^{N+1}-1} \langle k|\psi\rangle \sigma_x^{(i)}|k\rangle, \quad (16)$$

thus reducing our problem to that of finding an efficient way to multiply the basis vectors (6) by $\sigma_x^{(i)}$. Since the matrix $\sigma_x^{(i)}$ has the effect of flipping the i -th spin, one has

$$\sigma_x^{(i)}|k_N, \dots, k_i, \dots, k_0\rangle = |k_N, \dots, \bar{k}_i, \dots, k_0\rangle$$

where $\overline{k}_i = 1$ if $k_i = 0$ and $\overline{k}_i = 0$ if $k_i = 1$. Multiplication by $\sigma_x^{(i)}$, therefore, replaces the k -th component of $|\psi\rangle$ (where $k = k_0 + \dots + 2^i k_i + \dots + 2^N k_N$) with the k' -th component (where $k' = k_0 + \dots + 2^i \overline{k}_i + \dots + 2^N k_N$) and vice-versa. In binary representation, the numbers k and k' differ by a single bit (the i -th bit) and one can therefore obtain k' from k using Fortran intrinsic functions. Specifically, we used the XOR-function (exclusive or) to flip the i -th bit of the k -th state. Multiplication by $\sigma_z^{(i)}$ can be similarly implemented.

After determining the evolved density (13), we traced out the bath degrees of freedom to obtain the reduced density (14). As indicators of quantum coherence, we chose the polarisation and entropy of the central spin defined respectively as

$$\vec{P}(t) = \text{Tr}[\rho_0(t)\vec{\sigma}] \quad (17)$$

and

$$S_0(t) = -\text{Tr}[\rho_0(t) \ln \rho_0(t)] = -\frac{1}{2} \ln \left(\frac{1 - P^2}{4} \right) - \frac{P}{2} \ln \left(\frac{1 + P}{1 - P} \right). \quad (18)$$

Here $P = |\vec{P}|$ denotes the modulus of the polarisation vector \vec{P} . Note that (17) contains as much information as the reduced density itself. In fact (14) can be expressed in terms of \vec{P} via

$$\rho_0(t) = \frac{1}{2} (\mathbf{1} + \vec{P}(t) \cdot \vec{\sigma}).$$

4 Dynamics of the central spin

Here we examine the effects of intra-environmental couplings on the dynamics of the central spin. We consider the antiferromagnetic and the ferromagnetic cases separately. High temperature results apply only to the case where the spin-bath represents true physical spins.

4.1 Antiferromagnetic interactions

To evaluate the effect of antiferromagnetic interactions we calculated the dynamics of the central spin for values of λ ranging from $\lambda = 0$ (uncoupled spins) to $\lambda = 10$ (strong coupling). As a point of reference, note that in the absence of *subsystem-environment* coupling $P_z(t)$ - initially one - undergoes periodic fluctuations to slightly smaller values. The components $P_x(t)$ and

$P_y(t)$ - initially zero - oscillate about zero with the same period and similar small amplitude.

The entropy (18) is shown in Fig. 1. Figs. 2, 3, and 4 show components of the polarisation (17). In the figures, each curve corresponds to a

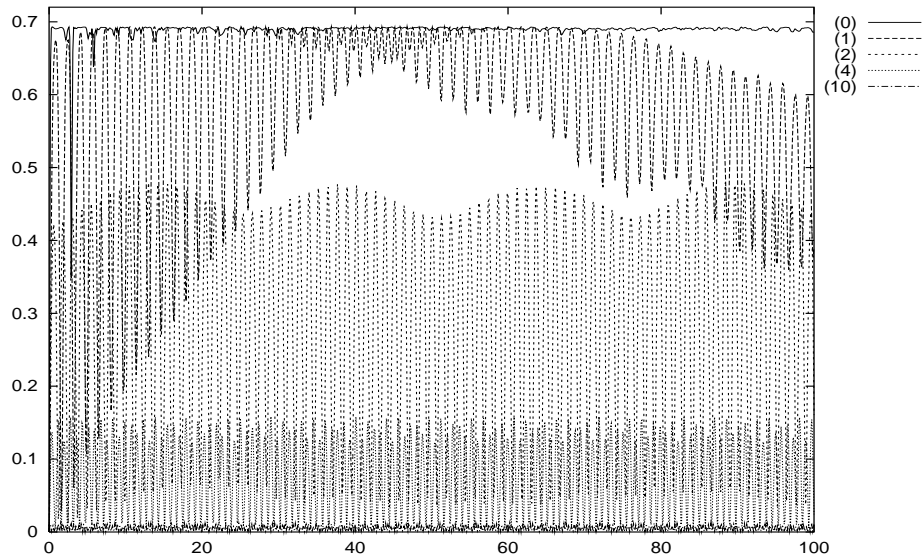


Figure 1: $S_0(t)$ versus $\omega_c t$ (14 bath spins).

different value of the intra-environmental coupling λ (reported in parenthesis to the right). The thermal average was computed for a bath at temperature $kT = 0.02$. The results shown are for $N = 14$ but are also representative of smaller baths with even numbers of spins (i.e., 8, 10 and 12). The time scale considered is long enough for the system to attain its asymptotic condition as can be seen from Fig. 5 which shows the entropy of the central spin on a much longer time scale (data obtained for $N = 10$ spins).

When $\lambda = 0$ (i.e., bath spins non-interacting), the central spin undergoes rapid decoherence, with the polarisation quickly falling to zero and the entropy $S_0(t)$ simultaneously approaching the maximum value $S_0^{max} = \ln(2) \simeq 0.693147\dots$. As λ increases, however, the entropy $S_0(t)$ tends to progressively smaller asymptotic values and the components of the polarisation vector approach the dynamics of a central spin evolving in isolation. In other words, *the existence of a strong interaction among bath spins suppresses*

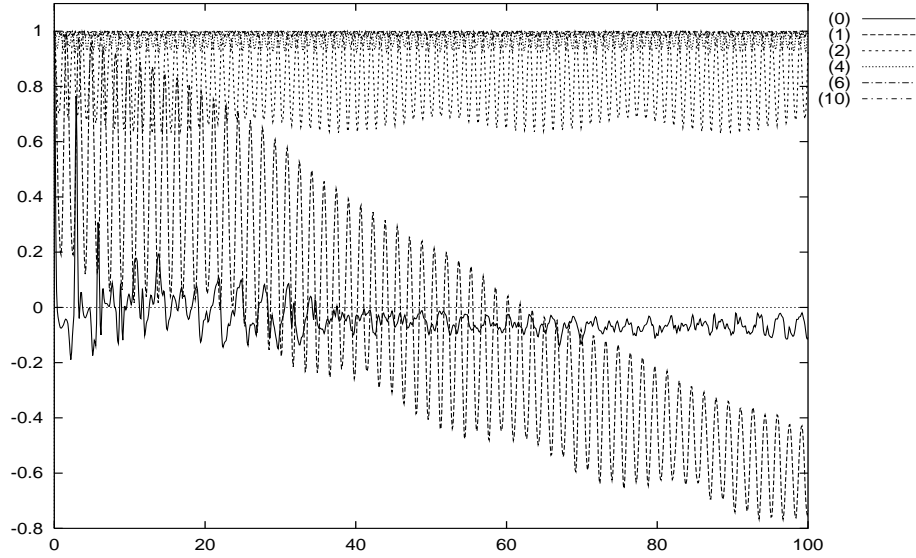


Figure 2: $P_z(t)$ versus $\omega_c t$ (14 bath spins).

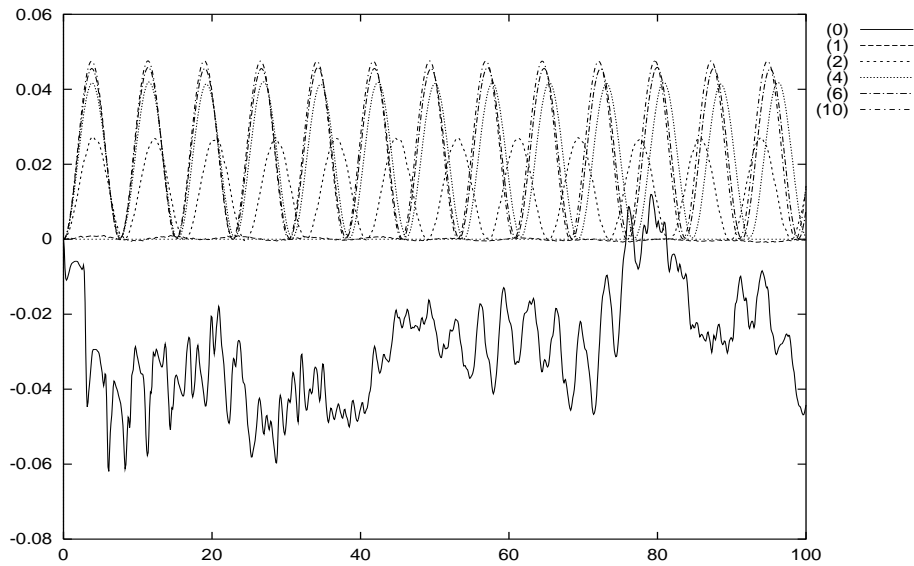


Figure 3: $P_x(t)$ versus $\omega_c t$ (14 bath spins).

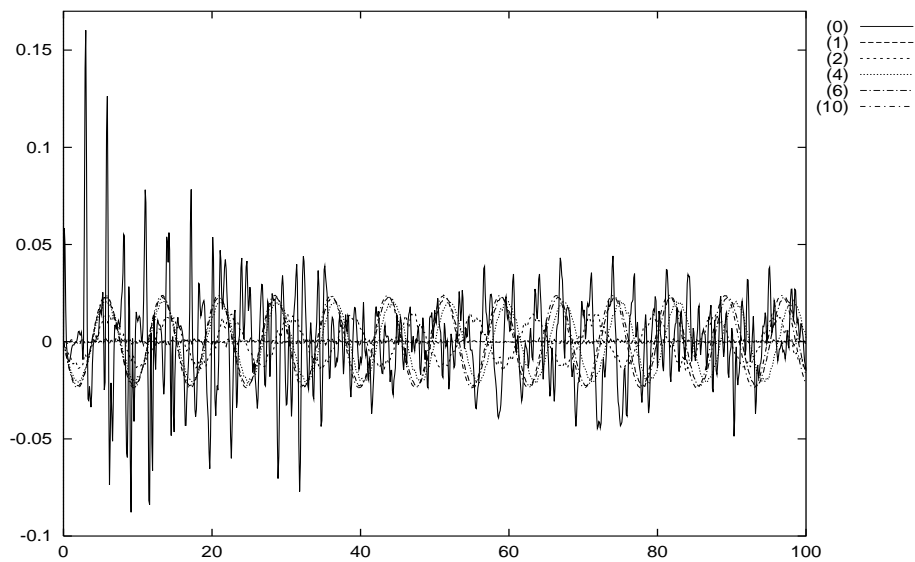


Figure 4: $P_y(t)$ versus $\omega_c t$ (14 bath spins).

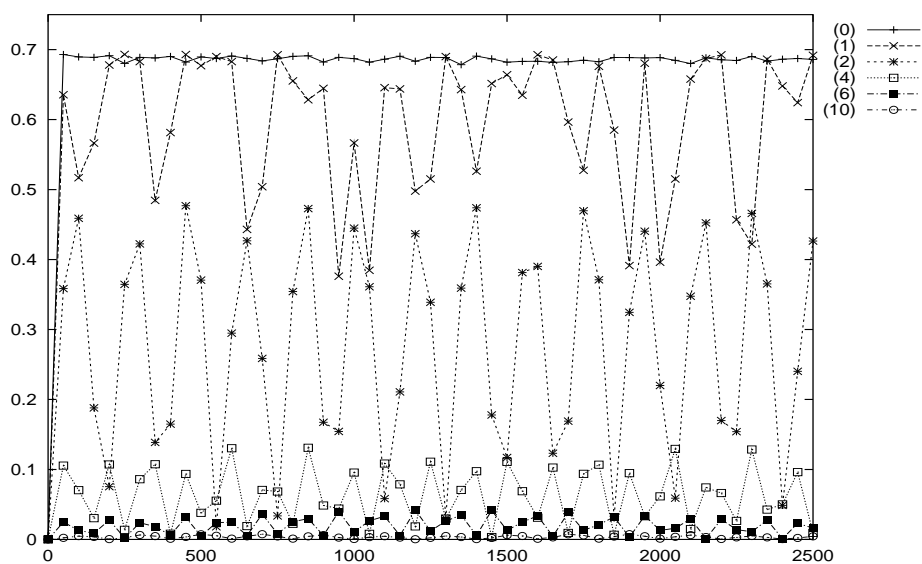


Figure 5: $S_0(t)$ versus $\omega_c t$ (10 bath spins).

environmental decoherence.

This apparently puzzling result is a straightforward consequence of the fact that strong interactions between bath spins produce an almost complete decoupling of the central spin from the bath. This can be verified by considering the thermal average of the interaction Hamiltonian (4), defined as

$$\langle H_I(t) \rangle = \sum_{n=1}^{2^N} \langle \psi_n(t) | H_I | \psi_n(t) \rangle e^{-E_n/kT} / Q. \quad (19)$$

Note that $\langle H_I(t) \rangle$, rather than λ_0 , is the physically relevant quantity determining the strength of the interaction. In fact, the interaction may be small even if λ_0 is large. The evolution of $\langle H_I(t) \rangle$ is displayed in Fig. 6, which shows that as λ increases the effective interaction of the central spin with the bath tends to zero (data obtained for 10 spins). Quantitatively, $\langle H_I \rangle$

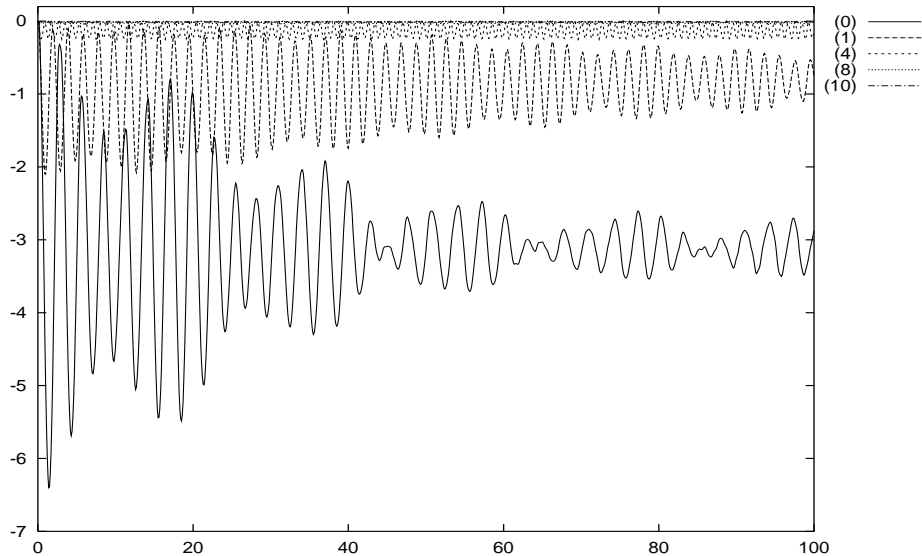


Figure 6: Thermal average $\langle H_I \rangle$ of the interaction Hamiltonian versus $\omega_c t$ (10 bath spins).

averaged over the time interval $[0 : 2500\omega_c^{-1}]$ decreases from $\overline{\langle H_I \rangle} = -3.07$ for $\lambda = 0$ to $\overline{\langle H_I \rangle} = -0.01$ for $\lambda = 10$.

There is a simple explanation for the observed behaviour of the average

interaction term (19). Define the total bath spin

$$\vec{\Sigma} = \sum_{i=1}^N \vec{\sigma}^{(i)}, \quad (20)$$

(i.e., $\Sigma_x = \sum_{i=1}^N \sigma_x^{(i)}$ etc.) and rewrite the interaction Hamiltonian (4) and bath Hamiltonian (3) in the suggestive forms

$$H_I = \lambda_0 \sigma_x^{(0)} \Sigma_x$$

and

$$H_B = \frac{\lambda}{2} [\Sigma_x^2 - N\mathbf{1}] + \beta \Sigma_x + \sum_{i=1}^N \frac{\omega_i}{2} \sigma_z^{(i)}. \quad (21)$$

Eq. (21) shows that for $\lambda \gg \omega_c$ the bath Hamiltonian takes the approximate form

$$H_B = \frac{\lambda}{2} [\Sigma_x^2 - N\mathbf{1}] + O(\lambda^0) \quad (22)$$

which is essentially proportional to Σ_x^2 . Thus for large values of λ the bath eigenstates (10) must be approximate eigenvectors of Σ_x and those of lowest energy must correspond to the eigenstates of Σ_x with zero eigenvalue. (That many such eigenstates exist is a consequence of the fact for every value of the macroscopic variable Σ_x there are many corresponding microstates). Thus, for low temperature and large λ the relevant diagonal and off-diagonal matrix elements of the environment coupling operator Σ_x will be zero.

These conclusions are confirmed by the numerical evaluation of the expectation values of Σ_x on the bath eigenstates (10). Fig. 7 reports $\langle \phi_n^{(B)} | \Sigma_x | \phi_n^{(B)} \rangle$ as a function of the index n which orders the eigenstates $|\phi_n^{(B)}\rangle$ in ascending energy (data obtained for $N = 10$ so n runs from 1 to 1024). Data are shown for $\lambda = 0$ and $\lambda = 10$. For $\lambda = 0$ the expectation values of Σ_x are small but non-zero (this is more evident in the inset, which displays the data for the 100 lowest energies). For $\lambda = 10$ the expectation value of Σ_x has a sort of step-like behaviour and attains relatively large values for high-energy bath eigenstates. At low temperatures only low-energy states matter and for these $\langle \phi_n^{(B)} | \Sigma_x | \phi_n^{(B)} \rangle$ is orders of magnitude smaller than for the $\lambda = 0$ case (see inset in Fig. 7). This effect can be quantified by computing the quantity

$$\langle \Sigma_x \rangle = \frac{1}{20} \sum_{n=1}^{20} \langle \phi_n^{(B)} | \Sigma_x | \phi_n^{(B)} \rangle. \quad (23)$$

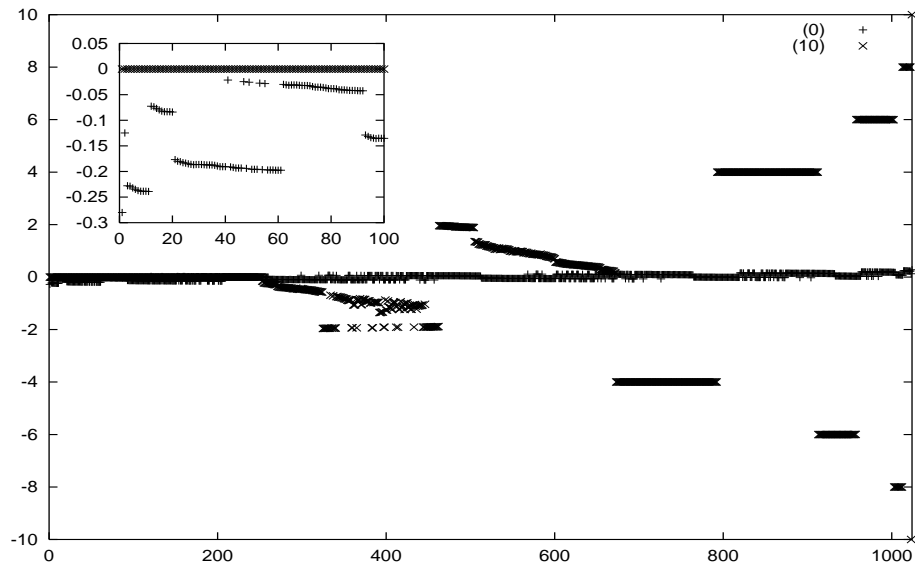


Figure 7: Expectation value $\langle \phi_n^{(B)} | \Sigma_x | \phi_n^{(B)} \rangle$ versus n for $\lambda = 0$ and $\lambda = 10$. The stacked inset shows on a larger scale the first 100 values. The data were obtained for a 10-spin bath.

One finds

$$\langle \Sigma_x \rangle = \begin{cases} -0.161951 & \text{for } \lambda = 0 \\ -6.0 \cdot 10^{-5} & \text{for } \lambda = 10 \end{cases} \quad (24)$$

for $N = 10$ spins which is indeed small for strong coupling.

4.1.1 High temperature limit

Fig. 7, for $\lambda = 10$, shows that the expectation values of Σ_x are large for high-energy bath states. Populations in these states are zero at low temperatures but increase with temperature. The thermal average interaction (19) will therefore also increase with temperature, effectively coupling the central spin to its bath. As a consequence, one can expect that the self-interacting bath will behave more and more like an ordinary bath of uncoupled spins when the temperature is raised. Fig. 8 shows the time behaviour of the central spin entropy for a bath of 10 coupled spins (with $\lambda = 10$) at various temperatures. Entropy increases monotonically with temperature, progressively

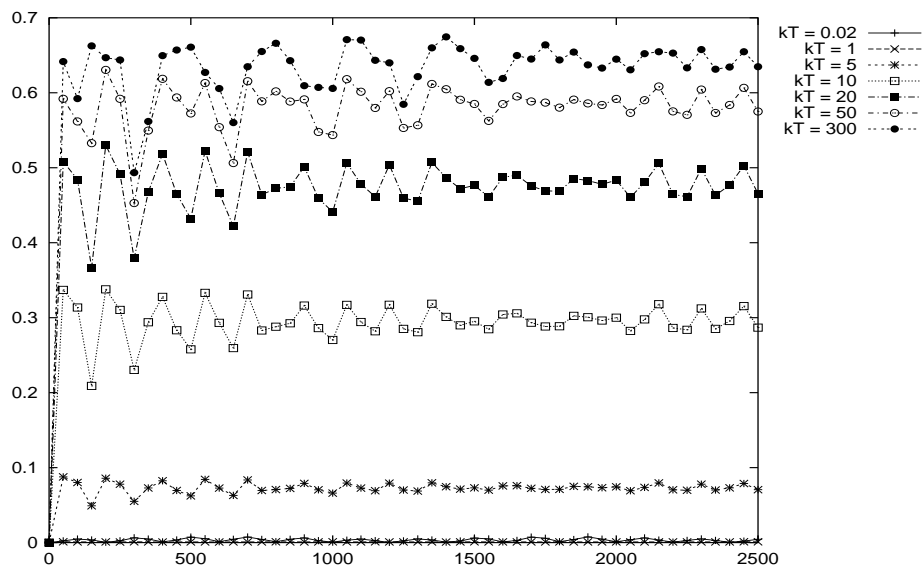


Figure 8: S_0 versus $\omega_c t$ for $\lambda = 10$ for various temperatures of the bath (10 bath spins).

approaching the behaviour characteristic of the uncoupled bath. However,

even at high temperature ($kT = 300$) the entropy remains lower than for a bath of uncoupled spins: this shows that even at high temperatures the spin-spin coupling has a reductive effect on decoherence. These features are confirmed in Fig. 9. Raising the temperature lowers the asymptotic value of

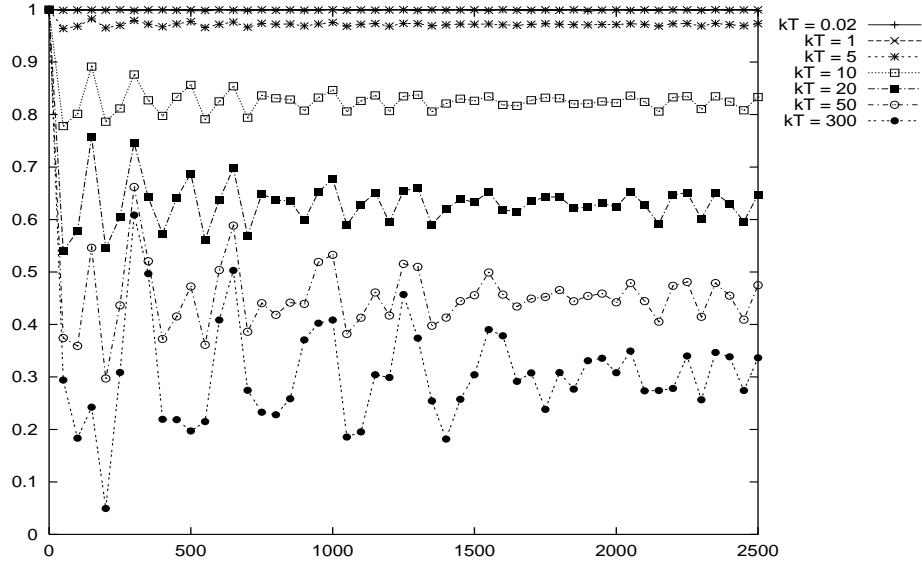


Figure 9: P_z versus $\omega_c t$ for $\lambda = 10$ for various temperatures of the bath (10 bath spins).

$P_z(t)$ which however never becomes zero.

In summary, at low temperatures the strong intra-environmental interactions force the bath spins to align in an antiferromagnetic state of zero moment and behave like a single giant spin decoupled from the central spin. As the temperature is raised thermal fluctuations eliminate the spin alignment and switch on the subsystem-environment coupling, making the self-interacting bath behave more like an ordinary bath of uncoupled spins.

4.1.2 Odd numbers of spins

So far we have considered the behaviour of a central spin coupled to a bath composed of an *even* number of spins. To complete the discussion of antiferromagnetic interactions, we briefly mention a last feature of the self-interacting

spin bath - namely modifications which appear for baths with an *odd* number of spins.

Figs. 10 and 11 show $S_0(t)$ and $P_z(t)$ for $N = 11$. Similar behaviour was obtained with baths of 5, 7, and 9 spins. Only $\lambda = 0, 1$ and 10 are shown because the curves for λ greater than 1 overlap. The data show

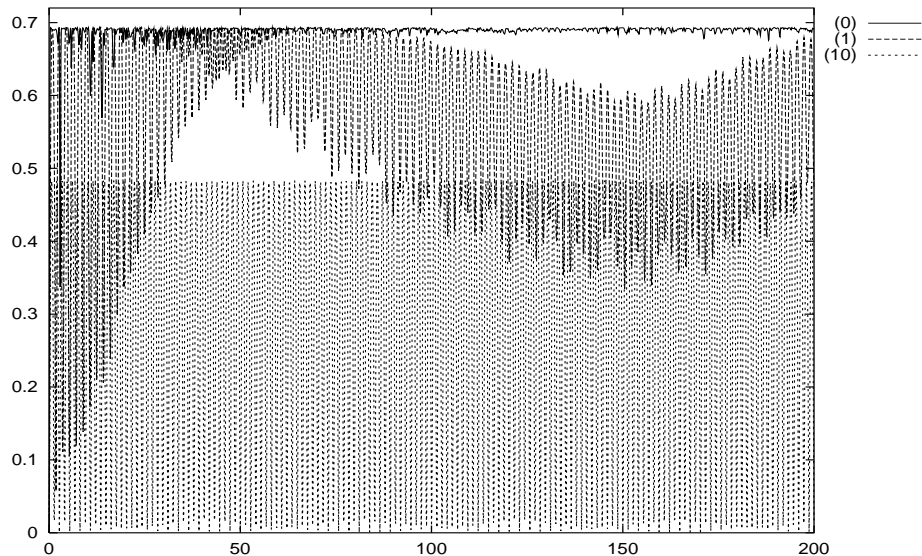


Figure 10: S_0 versus $\omega_c t$ (bath composed of 11 spins).

that, regardless of whether the number of bath spins is even or odd, $S_0(t)$ is a decreasing function of the intra-environmental coupling. However, for N odd, the average value of the entropy decreases less than for N even and oscillates more (compare Figs. 10 and 1). Polarisation behaves similarly. As shown in Fig. 11, when the intra-environmental interactions are strong, $P_z(t)$ oscillates around the value $P_z(t) \simeq 0.8$ for baths with odd number of spins, whereas one has $P_z(t) \simeq 1$ for a bath with an even number of spins. Nor do the oscillations die on a longer time scale: in fact, numerical calculations performed via the exact diagonalisation of the Hamiltonian show oscillatory behaviour persisting on time scales an order of magnitude longer than that in Figs. 10 and 11. Thus intra-environmental interactions have the effect of suppressing decoherence regardless of how many spins compose the bath; however, this effect is more marked if the bath is composed of an even, rather

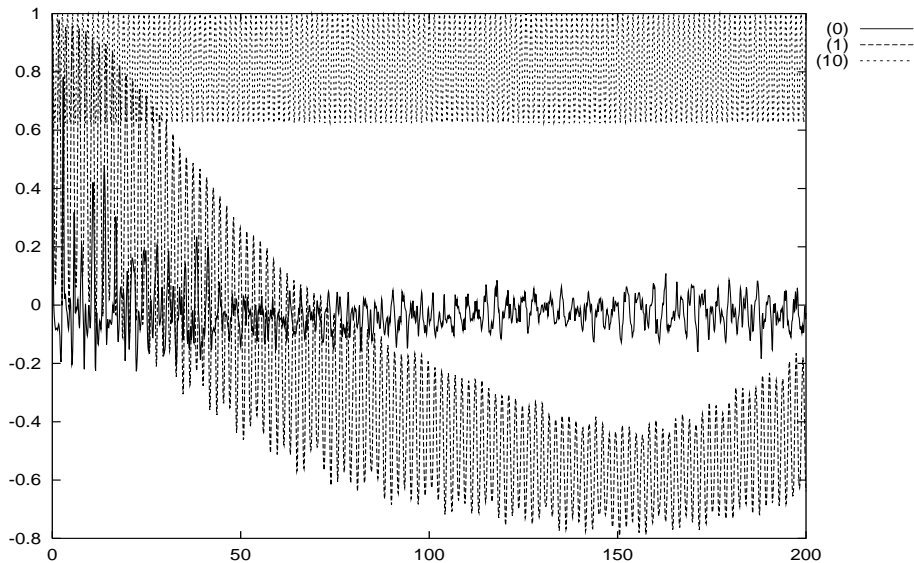


Figure 11: P_z versus $\omega_c t$ (bath composed of 11 spins).

than an odd, number of spins.

The oscillations of entropy and polarisation are also displayed in the strength of the interaction between the central spin and its bath. Fig. 12 shows the thermal average of the interaction Hamiltonian (4). Comparing Fig. 12 with Fig. 6, it is evident that the interaction between the central spin and bath is weaker for N even than N odd. Computing the parameter (23) for a bath of 11 spins gives

$$\langle \Sigma_x \rangle = \begin{cases} -0.19180 & \text{for } \lambda = 0 \\ -4.97 \cdot 10^{-3} & \text{for } \lambda = 10 \end{cases} . \quad (25)$$

Comparing Eq. (24) with Eq. (25) shows that $\langle \Sigma_x \rangle$ is a decreasing function of λ for baths of both even and odd numbers of spins but $\langle \Sigma_x \rangle$ for $\lambda = 10$ is two orders of magnitude larger for the 11-spin bath than for the 10-spin bath. Table 1 shows that as N increases $\langle \Sigma_x \rangle$ (for $\lambda = 10$) decreases. The even-odd difference is thus a finite-size effect which should vanish in the thermodynamic limit.

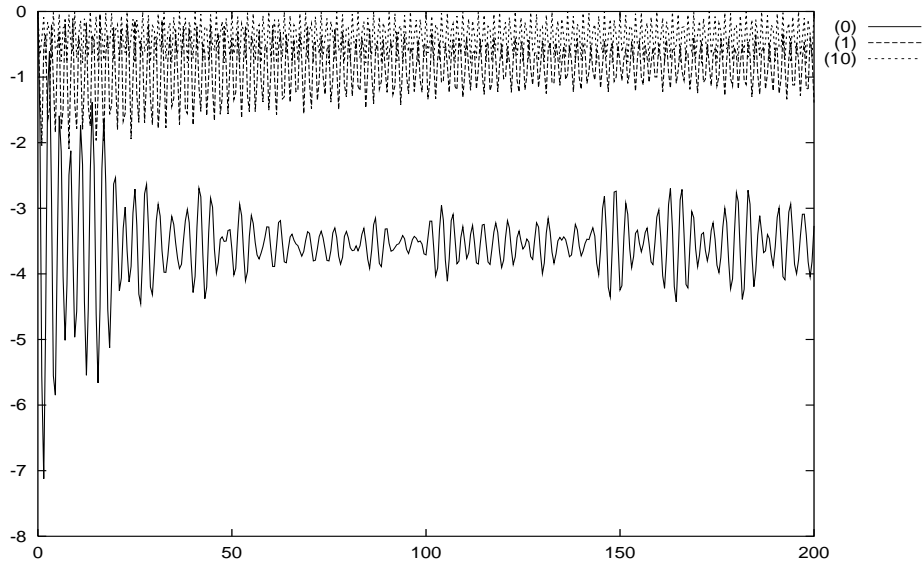


Figure 12: Thermal average $\langle H_I \rangle$ of the interaction Hamiltonian versus $\omega_c t$ (baths of 11 spins).

Number of bath spins	$\langle \Sigma_x \rangle$ for $\lambda = 10$
7	-0.011147
9	-0.006724
11	-0.004967

Table 1: $\langle \Sigma_x \rangle|_{\lambda=10}$ as a function of N

4.2 Ferromagnetic interactions

The entropy for the ferromagnetic case is shown in Fig. 13. The data were obtained for a bath of 10 spins; we use a semi-logarithmic scale to distinguish the curve for $\lambda = -2$ from the x -axis. We do not show data for values of $\lambda < -2$ because they overlap. The behaviour of the entropy is similar in the

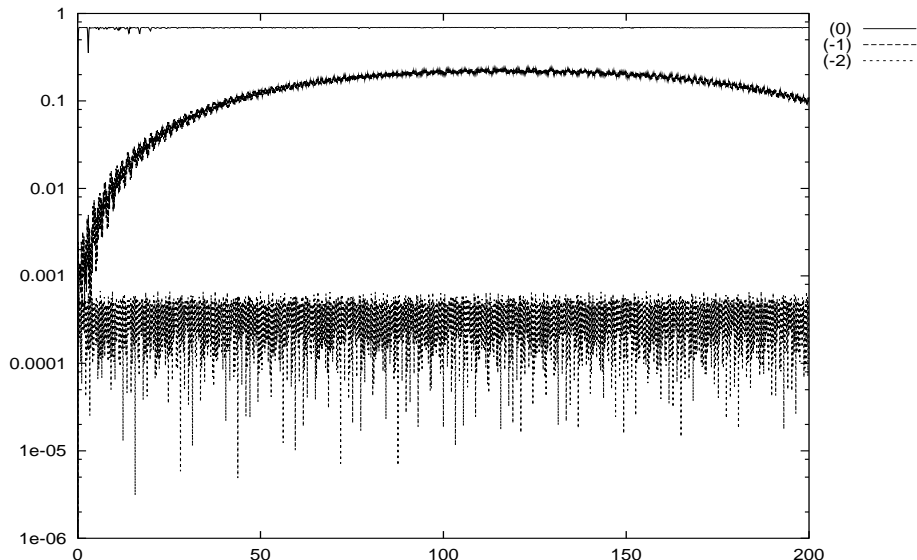


Figure 13: $\ln(S_0)$ versus $\omega_c t$ (10 spin bath).

ferromagnetic and antiferromagnetic cases; the only significant difference is that in the ferromagnetic case a suppression of the entropy can be achieved with weaker intra-environmental interactions.

The most relevant difference between antiferromagnetic and ferromagnetic baths emerges when one considers the behaviour of the polarisation vector (17) shown in Figs. 14, 15, and 16. We have chosen a time scale appropriate to the fast oscillations of the polarisation components (but long enough to be representative of the long-time behaviour of $\vec{P}(t)$). For $\lambda \leq -2$ the components of the polarisation vector assume a strongly oscillatory behaviour. This is consistent with the suppression of entropy since entropy depends only on the norm of the polarisation vector which can stay close to unity even if individual components of \vec{P} oscillate in time. Such polarisation

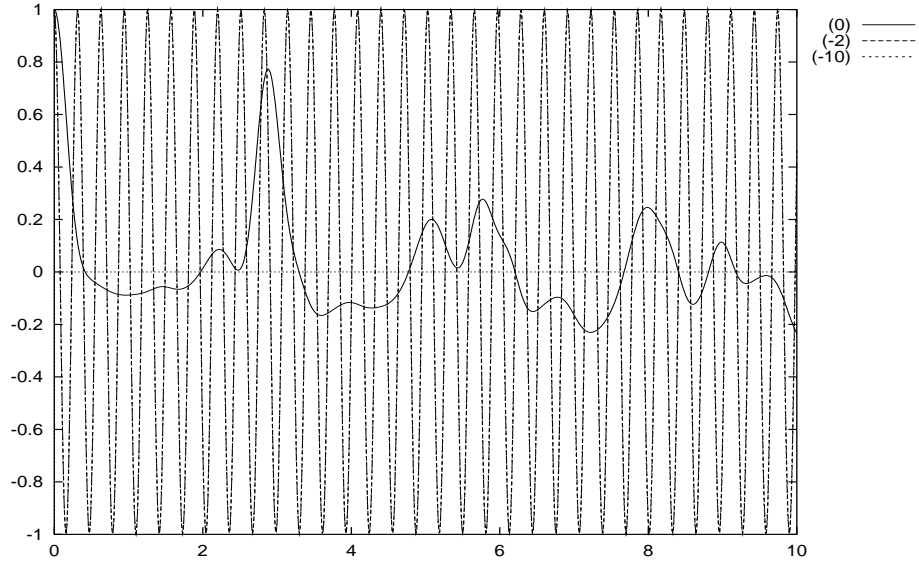


Figure 14: P_z versus $\omega_c t$ (10 spin bath).

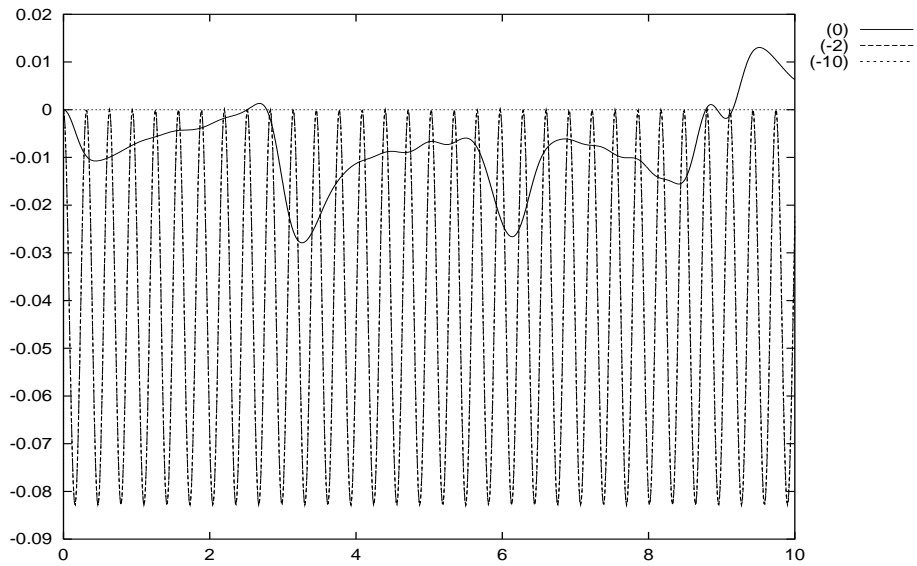


Figure 15: P_x versus $\omega_c t$ (10 spin bath).

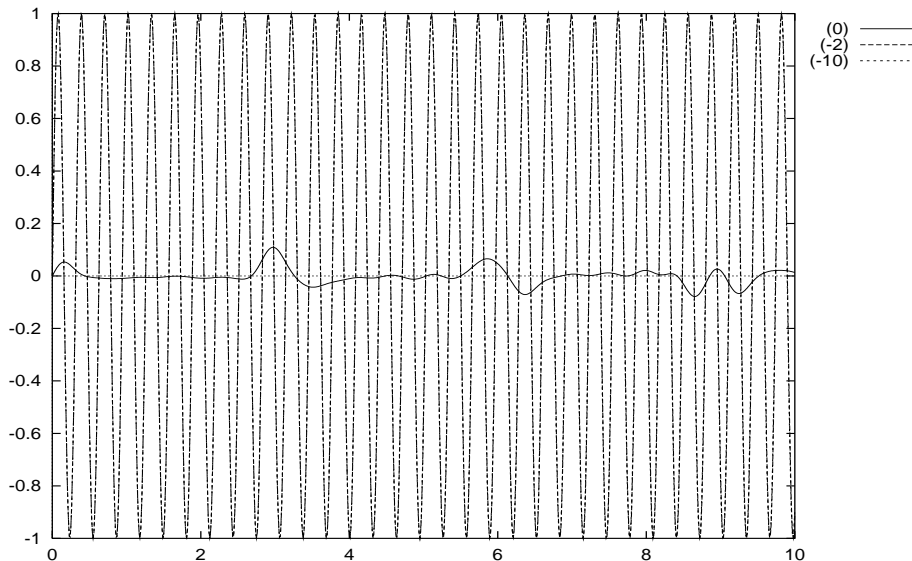


Figure 16: P_y versus $\omega_c t$ (10 spin bath).

dynamics, however, is very different from that observed in the antiferromagnetic case where $P_z(t) \simeq 1$ and $P_x(t) \simeq P_y(t) \simeq 0$ at all times. Term (19) is not negligible for ferromagnetic interactions, as can be seen in Fig. 17, where we represent the thermal average of the interaction Hamiltonian as a function of time. For $\lambda \leq -2$, the interaction term $\langle H_I(t) \rangle$ becomes almost independent of the strength of the spin-spin coupling and oscillates around a non-zero value.

This behaviour can be explained by writing the bath Hamiltonian in the form (21) and by observing that in the limit of strong ferromagnetic interaction

$$H_B = -\frac{|\lambda|}{2} [\Sigma_x^2 - N\mathbf{1}] + O(\lambda^0). \quad (26)$$

Note that the antiferromagnetic and ferromagnetic Hamiltonians (22) and (26) are identical but with opposite sign. The bath eigenstates of lowest energy are eigenstates of Σ_x in both cases, but with $\langle \phi_n^B | \Sigma_x | \phi_n^B \rangle \simeq 0$ in the antiferromagnetic case and $|\langle \phi_n^B | \Sigma_x | \phi_n^B \rangle| \gg 1$ in the ferromagnetic case. This is confirmed by Fig. 18, which represents $\langle \phi_n^B | \Sigma_x | \phi_n^B \rangle$ as a function of the index n . Not surprisingly, the distribution of points for $\lambda = -10$ is almost the reverse of the distribution for $\lambda = 10$ shown in the corresponding Fig. 7.

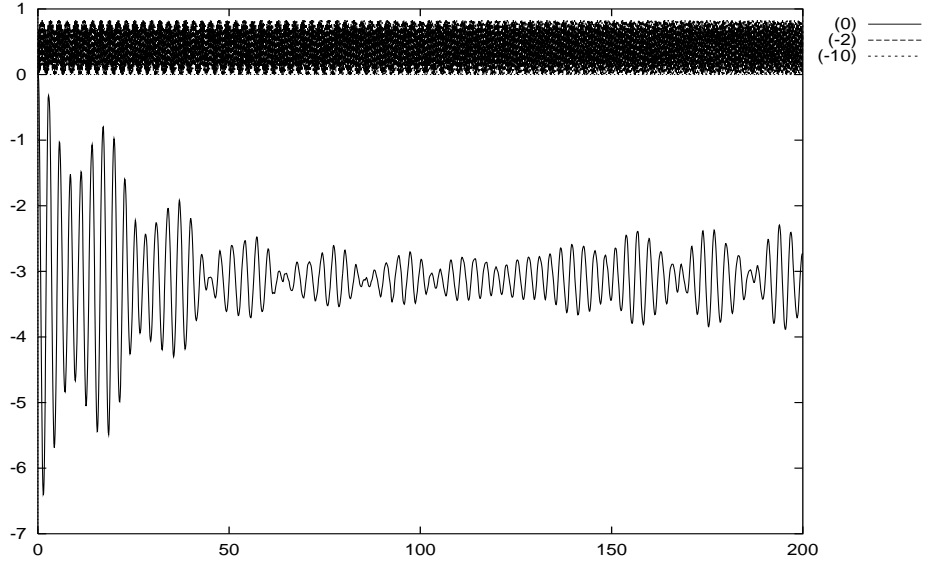


Figure 17: $\langle H_I \rangle$ versus $\omega_c t$ (10 spin bath).

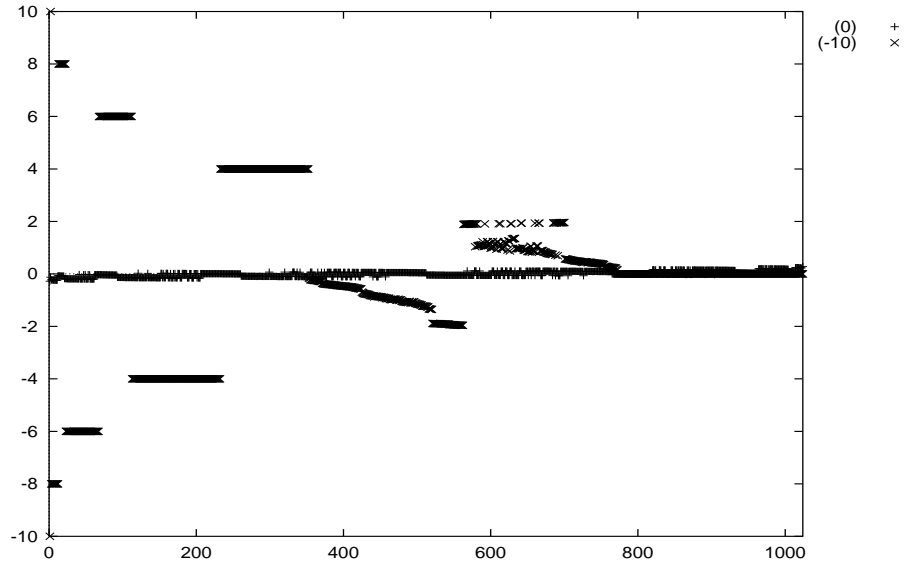


Figure 18: Expectation value $\langle \phi_n^{(B)} | \Sigma_x | \phi_n^{(B)} \rangle$ versus n for $\lambda = 0$ and $\lambda = -10$ (10 spin bath).

Consequently the coupling term (19) is significantly larger for a ferromagnetic bath than it is for an antiferromagnetic one. Thus, diagonal matrix elements of the coupling operator Σ_x are large while off-diagonal matrix elements are again zero.

It is important to note that the oscillations of the average interaction Hamiltonian (19) are synchronous with those of $P_x(t)$: more precisely

$$\beta'(t) = \langle H_I(t) \rangle / P_x(t)$$

is practically constant in time and, for $\lambda \leq -2$, it takes the value

$$\beta' \simeq -10$$

regardless of the strength of the spin-spin coupling. The value of β' is easily explained. The matrix element $\langle \phi_1^B | \Sigma_x | \phi_1^B \rangle$ corresponding to the lowest energy bath eigenstate is -10 while that of the next lowest is 10. However, the energy gap between these states is .2 leading to a population ratio $p_2/p_1 \sim 10^{-5}$ at $kT = .02$. Hence, the lowest energy state is the only one populated (in sharp contrast to the antiferromagnetic case) and its Σ_x eigenvalue is -10. This also explains why decoherence is more easily suppressed in the ferromagnetic case.

Thus the central spin interacts with the bath through

$$H_I^{eff} = \beta' \sigma_x^{(0)}, \quad (27)$$

and the evolution of the central spin is dictated by Hamiltonian (2) with a renormalised β parameter:

$$\beta \rightarrow \tilde{\beta} = \beta + \beta' \simeq -10. \quad (28)$$

Solving the Heisenberg equations for the renormalised central spin with initial conditions $P_z(0) = 1$, $P_x(0) = P_y(0) = 0$ gives

$$\begin{aligned} P_x(t) &= \frac{2\tilde{\beta}\omega_0}{\Omega^2} (1 - \cos \Omega t) \\ P_y(t) &= -\frac{2\tilde{\beta}}{\Omega} \sin \Omega t \\ P_z(t) &= 1 - \frac{4\tilde{\beta}^2}{\Omega^2} (1 - \cos \Omega t) \end{aligned} \quad (29)$$

where $\Omega = \sqrt{\omega_0^2 + 4\tilde{\beta}^2}$. Comparing Eq. (29) with the actual data shows that (27) is correct. Figs. 14, 15 and 16 do not show $\vec{P}(t)$ predicted by Eq. (29) because of overlapping of the various curves.

We therefore conclude that the only effect that a low temperature bath with internal ferromagnetic interactions has on the central spin is a renormalisation (28) of the β parameter in the Hamiltonian (2) (i.e., a Lamb shift). In both the antiferromagnetic and the ferromagnetic cases, therefore, when intra-environmental interactions are strong the dynamics of the central spin is almost autonomous from that of the bath and is dictated by a Hamiltonian of the form (2).

As a last remark on the ferromagnetic case, we observe that the dynamics of the central spin is unaffected by whether the bath is composed of an even or odd number of spins.

5 Summary and Conclusions

In this work we considered a spin 1/2 subsystem coupled to a low-temperature bath of interacting spin-1/2 modes. We focussed attention on the effects of antiferromagnetic and ferromagnetic intra-environmental interactions on decoherence. In both cases strong intra-environmental interactions suppress decoherence by making the dynamics of the central spin almost autonomous from the bath itself. More precisely, strong antiferromagnetic couplings among bath spins make the average value of the subsystem-environment interaction Hamiltonian vanish, thereby making the central spin evolve with its unperturbed and uncoupled Hamiltonian. Strong ferromagnetic couplings among bath spins, on the other hand, cause a Lamb shift of the subsystem Hamiltonian but otherwise leave it to evolve in isolation.

These effects can be schematically explained by considering (1) with $H_I = SB$ where S and B are subsystem and bath operators. Now, the eigenstates of H_B are also eigenstates of B for strong intra-environmental coupling in our model. Hence the off-diagonal matrix elements of B in this eigenbasis are zero and so (1) cannot couple bath eigenstates. Since the initial states of the full system are proportional to bath eigenstates for initial conditions (11) it follows that the time evolved reduced density must be of the form

$$\rho_0(t) = \sum_n \frac{e^{-E_n/kT}}{Q} e^{-i(H_0+SB_n)t} \rho_0(0) e^{i(H_0+SB_n)t} \quad (30)$$

where B_n is the eigenvalue of B corresponding to eigenstate $|\phi_n^{(B)}\rangle$ of H_B . In the antiferromagnetic case we found that all relevant B_n were zero for strong intra-environmental coupling and hence the dynamics was free of decoherence. For the ferromagnetic case we found that only the lowest energy state was populated at low temperature and so only one term contributes to (30) and again the dynamics is coherent, but with a Lamb shift.

We expect similar effects to occur in more general baths of coupled anharmonic oscillators. The key issue as we have seen is what happens to the matrix elements of the spin-bath coupling Hamiltonian, in the eigenbasis of the bath, when bath self-interactions are turned on. To suppress decoherence the off-diagonal matrix elements must be small. Clearly in an integrable bath (i.e., no self-interaction) some off-diagonal matrix elements will be large due to selection rules. One would thus expect strong decoherence for integrable environments. In the case of chaotic environments it is known that the off-diagonal matrix elements are of order \hbar^{N-1} smaller than the diagonal matrix elements [26], where N is the number of environmental modes. Since Planck's constant is small and N is very large, the off-diagonal matrix elements for a chaotic environment are negligible. Hence, we expect at most a Lamb shift of the subsystem for each eigenstate of the bath and hence a reduced density like (30). If in addition the diagonal matrix elements (i.e. B_n) vary slowly with energy then at low temperatures we should obtain a reduced density

$$\rho_0(t) = e^{-i(H_0+SB_0)t} \rho_0(0) e^{i(H_0+SB_0)t} \quad (31)$$

where B_0 is a representative low energy diagonal matrix element of the coupling operator. Dynamics should therefore be coherent but (possibly) Lamb-shifted for systems interacting with low temperature chaotic environments.

Finally, returning to the specific case of an atomic impurity in a crystal at low temperature, consider the limit of strong phonon-phonon coupling. Since the Wigner functions of the bath eigenstates are nearly uniform over the energetically available phase space [7], energy is distributed over an enormous number of phonon modes. At low temperature, displacements from equilibrium of any phonon mode must therefore be small. Since coupling of an impurity to a phonon is through its displacement coordinate [22], this coupling will also be small. Thus, we expect diagonal and off-diagonal matrix elements of the Jahn-Teller interaction to be small and decoherence to be minimal. Impurity-crystal configurations which might have these attributes

include noble gas substitutional or interstitial impurities in diamond (which has strong phonon-phonon interactions [27]).

The authors gratefully acknowledge the financial support of the Natural Sciences and Engineering Research Council of Canada.

References

- [1] A. O. Caldeira and A. J. Leggett, *Ann. Phys. (N.Y.)* **149**, 374 (1983)
- [2] U. Weiss, *Quantum dissipative systems*, 2nd edition, (World Scientific, Singapore, 1999); A.J. Leggett, S. Chakravarty, A.T. Dorsey, M.P.A. Fisher, A. Garg and W. Zwerger, *Rev. Mod. Phys.* **59**, 1 (1987).
- [3] See N. V. Prokof'ev and P. C. E. Stamp, *Rep. Prog. Phys.* **63(4)**, 669 (2000) and references therein.
- [4] D. Braun, F. Haake and W.T. Strunz, *Phys. Rev. Lett.* **86**, 2913 (2001).
- [5] V.I. Arnold and A. Avez, *Ergodic problems of classical mechanics*, (Addison-Wesley, New York, 1989).
- [6] F. Haake, *Quantum signatures of chaos*, 2nd edition. Springer Verlag, Berlin (2001); M.V. Berry in *Chaotic behavior in quantum systems*, eds. G. Ioos, R.H.G. Helleman and R. Stora, (North-Holland, Amsterdam, 1983).
- [7] M.V. Berry, *Proc. Roy. Soc. Lond. A* **423**, 219 (1989)
- [8] J. Wilkie, P. Brumer, *J. Chem. Phys.* **107**, 4893 (1997); *Phys. Rev. Lett.* **67**, 1185 (1991)
- [9] H.-K. Lo, S. Popescu, and T. Spiller, *Introduction to quantum computation and information*, (World Scientific, Singapore, 1998)
- [10] P. Brumer, M. Shapiro, *Laser and Particle Beams*, **16**, 599 (1998)
- [11] V. Mujica, A. Nitzan, Y. Mao, W. Davis, M. Kemp, A. Roitberg, M. A. Ratner, *Adv. Chem. Phys.* **107**, 403 (1999)

- [12] See for example J.I. Cirac and P. Zoller, *Nature* **404**, 579 (2000); *Phys. Rev. Lett.* **74**, 4091 (1995)
- [13] A. Barenco, D. Deutsch, A. Ekert and R. Jozsa, *Phys. Rev. Lett.* **74**, 4083 (1995)
- [14] G.P. Berman, G.D. Doolen and V.I. Tsifrinovich, *Superlattices and Microstructures*, **27** 89 (2000).
- [15] J. Kempe, D. Bacon, D.A. Lidar and K.B. Whaley, *Phys. Rev. A* **63**, 042307 (2001)
- [16] R. P. Feynman, F. L. Vernon, Jr., *Annals of Physics* **24**, 118 (1963)
- [17] S. Nakajima, *Prog. Theor. Phys.* **20**, 948 (1958); R. Zwanzig, *J. Chem. Phys.* **33**, 1338 (1960); R. Zwanzig, in *Lectures in theoretical Physics*, Vol. 3, Interscience, New York (1961)
- [18] P. Gaspard and M. Nagaoka, *J. Chem. Phys.* **111**, 5668 (1999); A. Suárez, R. Silbey and I. Oppenheim, *J. Chem. Phys.* **97**, 5101 (1992); V. Romero-Rochin and I. Oppenheim, *J. Stat. Phys.* **53**, 307 (1988); *Physica A* **155**, 52 (1989); V. Romero-Rochin, A. Orsky and I. Oppenheim, *ibid.* **156**, 244 (1989); A.G. Redfield, *Adv. Magn. Reson.* **1**, 1 (1965)
- [19] J. Wilkie, *J. Chem. Phys.* **115**, 10335 (2001); *J. Chem. Phys.* **114**, 7736 (2001); *Phys. Rev. E* **62**, 8808 (2000)
- [20] See for example H.Wang, M. Thoss and W.H. Miller, *J. Chem. Phys.* **115**, 2991 (2001)
- [21] See for example M. Dube and P.C.E. Stamp, *Chem. Phys.* **268**, 257 (2001); N. Makri, *J. Chem. Phys.* **111**, 6164 (1999); J.S. Shao and P. Hanggi, *Phys. Rev. Lett.* **81**, 5710 (1998)
- [22] G. Davies, *Rep. Prog. Phys.* **44**, 787 (1981).
- [23] W. H. Press, S. A. Teukosky, W. T. Vetterling, B. P. Flannery, *Numerical Recipes in Fortran 77*, 2nd edition, Cambridge University Press, Cambridge (1992)
- [24] <http://www.caam.rice.edu/software/ARPACK/>

- [25] DOP853.f, E. Hairer, G. Wanner, <http://elib.zib.de/pub/elib/hairer-wanner/nonstiff/>
- [26] J. Wilkie and P. Brumer, *Phys. Rev. A* **55**, 43 (1997); M. Feingold and A. Peres, *Phys. Rev. A* **34**, 591 (1986); P. Pechukas, *Phys. Rev. Lett.* **51**, 943 (1983)
- [27] E. Anastassakis, A. Cantarero and M. Cardona, *Phys. Rev. B* **41**, 7529 (1990).